



Thermoelectric properties of indium-doped zinc oxide sintered in an argon atmosphere

Mati Ullah¹ · Wang Chunlei^{1,2} · Wen-Bin Su¹ · Abdul Manan³ · Arbab Safeer Ahmad⁴ · Ata Ur Rehman⁵

Received: 2 November 2018 / Accepted: 19 January 2019 / Published online: 29 January 2019
© Springer Science+Business Media, LLC, part of Springer Nature 2019

Abstract

Solid-state reaction (SSR) was used to synthesize samples of $(\text{Zn}_{1-x}\text{In}_x)\text{O}$, with $x = 0.05, 0.02, 0.01, 0.005$ and 0.00 respectively. All compositions were sintered in an argon atmosphere and their thermoelectric properties, phase constituents, and microstructures were investigated. Single-phase ceramic was formed for each composition with dense microstructure. In^{3+} doping lowered the electrical resistivity of ZnO and in the present study, lower value of electrical resistivity $\rho \sim 1.884 \text{ m}\Omega\text{-cm}$ and highest power factor ($P.F$) $\sim 4.660 \times 10^{-4} \text{ WK}^{-2} \text{ m}^{-1}$ at $693.4 \text{ }^\circ\text{C}$ respectively are obtained for the composition with $x = 0.02$. The electrical resistivities (ρ) of all compositions were regulated. The tuned and regulated (ρ) are expected to be helpful for future thermoelectric devices.

1 Introduction

In the last 4 decades, a subsequent and rapid growth of a revival ZnO as a semiconductor attained an inspiring potential candidate as energy applicant [1]. Thermoelectric materials are considered as useful tools for thermoelectric generation and are studied widely in the conversion of waste heat into useful energy. The main advantage of the thermoelectric materials is the conversion of waste heat energy to useful electrical energy [1]. Owing to the above-mentioned properties of thermoelectric devices; they are used in gas sensors, aerospace and military, etc. on large scale [2, 3].

Silicon and ZnO are the useful thermoelectric materials used for electric power generation [4, 5]. ZnO is one of the most suitable thermoelectric material which has higher Seebeck coefficient [6]. ZnO is a promising candidate that works at high-temperatures [7]. ZnO has unique physical and chemical properties. ZnO is an n -type semiconductor with a bandgap of $\sim 3.37 \text{ eV}$ at 300 K [8]. ZnO has higher Seebeck coefficient compare to other thermoelectric materials. For a good thermoelectric material, the higher Seebeck coefficient ($S.C$) and higher electrical conductivity (σ) are necessary. The higher $S.C$ and higher σ yield the highest $P.F$. One of the main disadvantages of ZnO is its high electrical resistivity. The room-temperature resistivity of ZnO is measured be $0.75 \times 10^6 \text{ }\Omega\text{-cm}$ at room temperature [9].

A small concentration of defects either in the form of vacancy, interstitial, antisite or addition of numerous dopants can significantly affect the conductivity in ZnO [10, 11]. In the recent past, Dutta et al. [12] completed a thorough study of the role of defects in tailoring electrical and optical properties of ZnO.

Material properties can be tuned by several techniques such as pressure, and chemical doping, etc. [13, 16]. The thermoelectric properties especial the electrical resistivity of ZnO has been reduced by donor dopants. Promising high temperature n -type thermoelectric properties of Al-doped ZnO were first brought to the public sight by Ohtaki et al. in 1996 [17]. Yang et al. [18] obtained a $P.F \sim 5.3 \times 10^{-4} \text{ Wm}^{-1} \text{ K}^{-2}$ at 750 K for Al-doped ZnO ceramics by field—assisted deforming technique. Augra et al. [19]

✉ Mati Ullah
mati.physics1@yahoo.com

✉ Wang Chunlei
wangcl@sdu.edu.cn

¹ School of Physics, Shandong University, Jinan 250100, People's Republic of China

² MOE State Key Laboratory of Crystal Materials, Shandong University, Jinan 250100, People's Republic of China

³ Department of Physics, University of Science & Technology Bannu, Bannu 28100, Khyber Pakhtunkhwa, Pakistan

⁴ Department of Physics, Islamia College Peshawar, Peshawar 25120, Khyber Pakhtunkhwa, Pakistan

⁵ Institute for Energy Transmission Technology and Applications School of Chemical Engineering, Northwest University, Xi'an 710069, People's Republic of China

obtained $\rho \sim 8.54 \times 10^{-5} \Omega \text{ m}$ for Al-doped ZnO films prepared by the pulsed laser deposition technique. Zhang et al. [20] obtained a $\rho \sim 2.14 \text{ m}\Omega\cdot\text{cm}$ at $1450 \text{ }^\circ\text{C}$ for Al-doped ZnO (AZO). Berardan et al. [21] studied the influence of the preparation conditions for Al-doped ZnO sintered in different atmospheres, i.e. N_2 and air. The electrical resistivity was lowered for the sample sintered in N_2 -atmosphere samples in comparison to sample sintered in air obtained $\rho \sim 2 \text{ m}\Omega\cdot\text{cm}$ and $P.F \sim 3.8 \times 10^{-4} \text{ WK}^{-2} \text{ m}^{-1}$ for the sample sintered in N_2 -atmosphere. Similarly, in another study, the electrical resistivity was observed to be much lower for thin films of Al-doped ZnO samples in Ar/H_2 atmosphere than air [22]. Recently, Mati et al. [23] obtained $\rho \sim 1.997 \text{ m}\Omega\cdot\text{cm}$ and $P.F \sim 4.818 \times 10^{-4} \text{ WK}^{-2} \text{ m}^{-1}$ for Al and In dually doped ZnO sintered using an inert argon atmosphere. More recently Mati et al. [24] obtained much lower $\rho \sim 1.550 \text{ m}\Omega\cdot\text{cm}$ and higher $P.F \sim 5.436 \times 10^{-4} \text{ WK}^{-2} \text{ m}^{-1}$ for Al and Ga co-doped ZnO sintered in an argon atmosphere. The achieved ρ and $S.C$ were lower in magnitudes but $P.F$ of the ceramics/compositions needs further improvement. This shows that the different dopants and sintering atmospheres lower the ρ and enhanced the $P.F$ ($S^2\sigma$) of ZnO based ceramics, but the reduction in ρ and enhancements in $P.F$ were limited. In_2O_3 is also studied to be a promising thermoelectric material [25].

In this article, the resistivity obtained for $\text{Zn}_{0.98}\text{In}_{0.02}\text{O}$ is much lower than the resistivities for other ZnO based materials studied previously and give a benchmark to the novelty of this study. Moreover, in this work attempts has been made to achieve a higher Seebeck coefficient ($S.C$) as well as a higher power factor ($P.F$) without disturbing thermal and electrical properties of the In^{3+} doped ZnO sintered in an argon atmosphere.

2 Experimental procedure (preparation and characterization of compositions)

The $(\text{Zn}_{1-x}\text{In}_x)\text{O}$ ($x = 0.05, 0.02, 0.01$ and 0.005) compositions were fabricated via conventional solid-state sintering route. The compositions were prepared by using ZnO (99.5%) and In_2O_3 (99%) as the raw materials. The raw materials were weighted in stoichiometric ratios and ball milled in polyethylene mill jars using ethanol as lubricant and zirconia balls as grinding media for 15 h. The obtained slurries were kept in a furnace tube (DGX-92438) at $\sim 105 \text{ }^\circ\text{C}$ overnight. Finally, the dry powders were sieved through $140 \mu\text{m}$ mesh, pressed into $10.0 \text{ mm} \times 2.0 \text{ mm} \times 2.0 \text{ mm}$ rectangular bars and sintered at $1450 \text{ }^\circ\text{C}$ in an argon atmosphere for 10 h. The phase analysis of the sintered samples was carried out using X-ray diffraction (XRD) technique (D8 Bruker Toshiba Japan) over an angular range $2\theta = 20^\circ - 80^\circ$ at a scan rate of $2^\circ/\text{mint}$ with a step size of 0.02° using $\text{Cu-K}\alpha$

radiation (wavelength $\lambda = 1.5418 \text{ \AA}$). The microstructure of all the sintered samples was examined using Scanning Electron Microscopy (SEM, Hitachi-S-480). The thermoelectric properties such as ρ , $S.C$, and $P.F$ were measured in a temperature range $100\text{--}700 \text{ }^\circ\text{C}$ using LSR-3 machine connected to a controlled computer system.

3 Results and discussions

Figure 1 shows the powder X-ray diffraction (XRD) patterns of all the sintered compositions in $(\text{Zn}_{1-x}\text{In}_x)\text{O}$ ($x = 0.05, 0.02, 0.01, 0.005$ and 0.00) series. The main peak of the XRD patterns of all the compositions matched the PDF# 70-2551 for the host ZnO that crystallized in hexagonal wurtzite structure with peaks positions shifting towards the larger interplanar spacing (d) due to the incorporation of the bigger cation of In^{3+} (0.80 \AA) for Zn^{2+} (0.74 \AA) [26] in the lattice of ZnO. No secondary phases were observed in the entire composition range showing the formation of a solid solution.

Figure 2a–d shows the morphology and topography of all the sintered compositions in $(\text{Zn}_{1-x}\text{In}_x)\text{O}$ ($x = 0.05, 0.02, 0.01$ and 0.005) series. For all compositions a dense microstructure with almost no porosity has observed. The elemental compositions of the samples obtained from the EDX analysis are shown in Fig. 3a–d. The results confirmed the presence of In, Zn, and O. The weight percentage of elemental composition of each ceramic composition changes from $x = 0.05$ to 0.005 are listed in Table 1.

The lattice parameters calculated from the XRD data for $(\text{Zn}_{1-x}\text{In}_x)\text{O}$ ($x = 0.05, 0.02, 0.01, 0.005$ and 0.00) ceramics

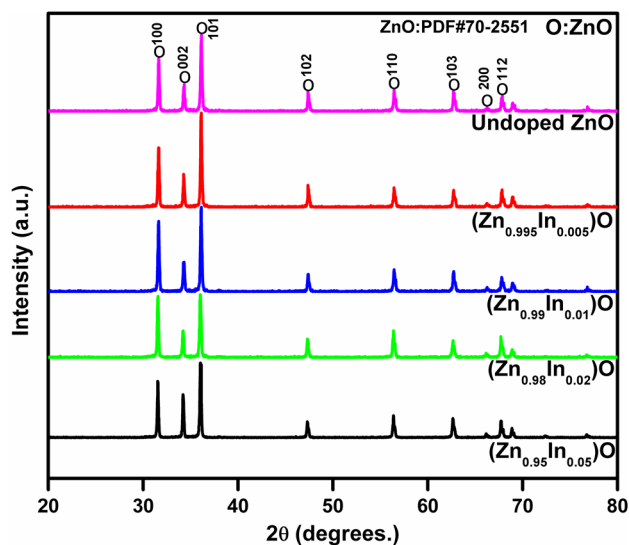


Fig. 1 Powder X-ray diffraction (XRD) of the nominal formula $(\text{Zn}_{1-x}\text{In}_x)\text{O}$, with $x = 0.05, 0.02, 0.01, 0.005$ and 0.00

Fig. 2 Scanning electron microscope (SEM) of the nominal formula $(\text{Zn}_{1-x}\text{In}_x)\text{O}$, with $x=0.05, 0.02, 0.01$ and 0.005

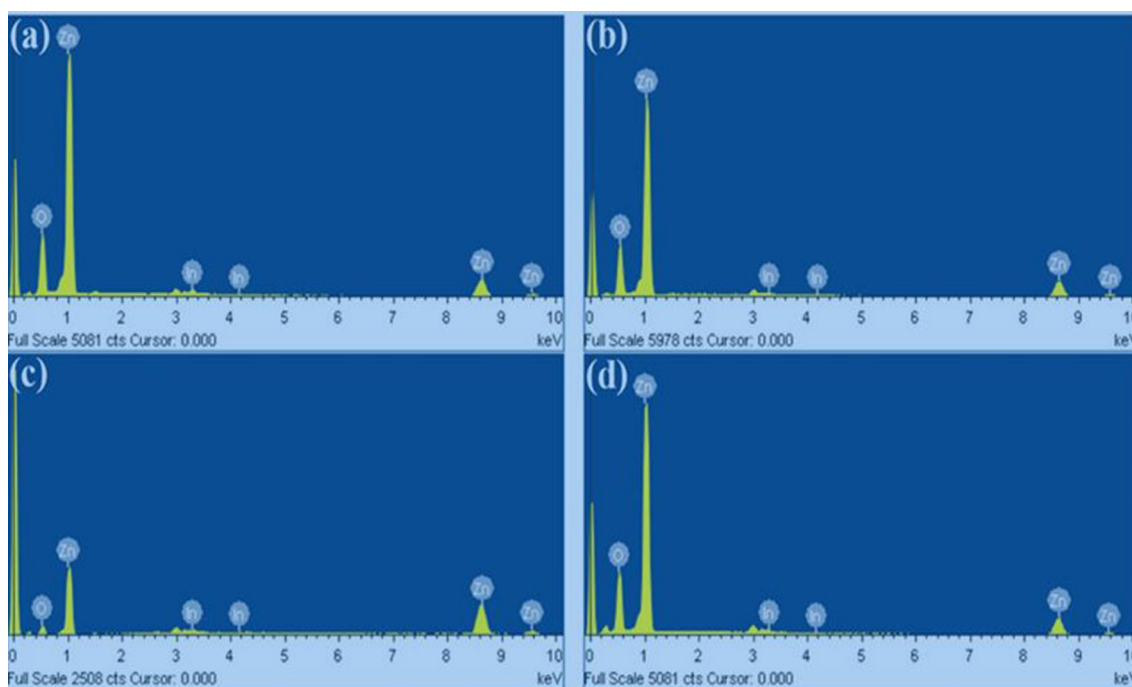
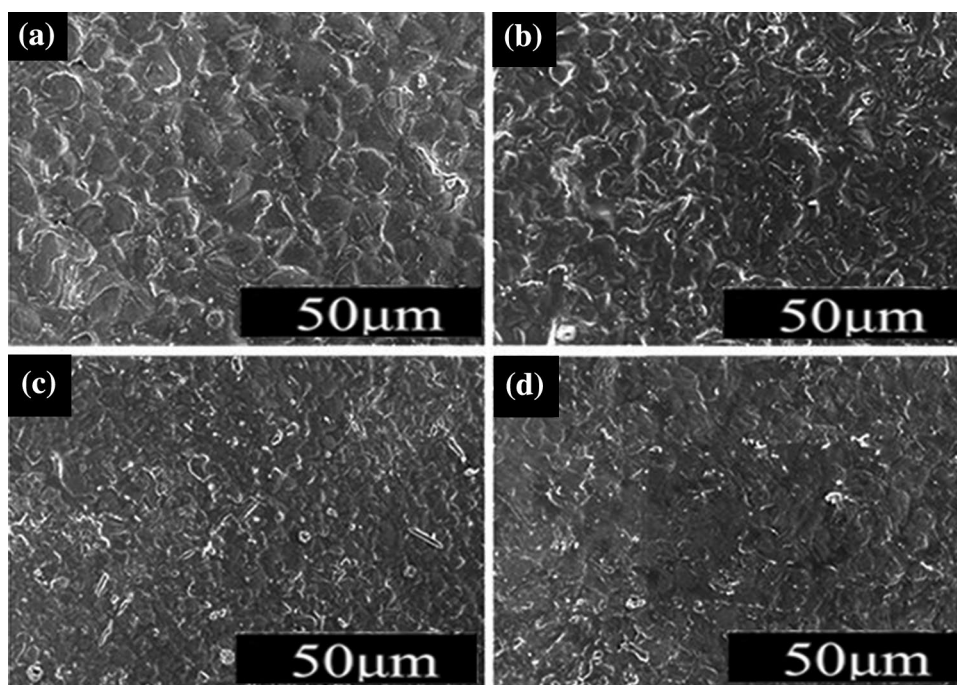


Fig. 3 Elemental analysis (EDX) of the nominal formula $(\text{Zn}_{1-x}\text{In}_x)\text{O}$, with $x=0.05, 0.02, 0.01$ and 0.005

are given in Table 2. The host ZnO had wurtzite structure having the lattice parameters of $a=b \neq c$, while the corresponding angles were $\alpha=\beta \neq \gamma$, where $\alpha=\beta=90^\circ$ and $\gamma=120^\circ$. In hexagonal wurtzite structure, the metal and oxygen ions direct facing lead to an increase in the “c” parameter [27]. The c/a ratio ~ 1.61 is very close to the c/a ratio ~ 1.633 of an ideal hexagonal wurtzite structure, indicating that single phase material

formed for each composition. The volume of the unit cell for hexagonal wurtzite structure can be calculated by [23],

$$V = 0.866a^2c \quad (1)$$

There exist a strong ionic bond between Zn and O_2 and the bond length (L) can be measured by using the relation [28],

Table 1 Wt% of Zn, In and oxygen for $(\text{Zn}_{1-x}\text{In}_x)\text{O}$, with $x=0.05$, 0.02, 0.01 and 0.005

Elements	Doping level $(\text{Zn}_{1-x}\text{In}_x)\text{O}$			
	$x=0.05$	$x=0.02$	$x=0.01$	$x=0.005$
Zn (mass %)	45.55 ^{0.5%}	43.24 ^{0.4%}	44.17 ^{0.455%}	45.46 ^{0.498%}
In (mass %)	00.94 ^{0.1%}	00.87 ^{0.009%}	00.57 ^{0.008%}	00.34 ^{0.004%}
O (mass %)	53.51 ^{0.4%}	55.89 ^{0.5%}	55.25 ^{0.488%}	54.20 ^{0.476%}
Total	100	100	100	100

Table 2 Relation between lattice parameter (a, c) and internal parameter (μ) for $(\text{Zn}_{1-x}\text{In}_x)\text{O}$, with $x=0.05$, 0.02, 0.01, 0.005 and 0.00

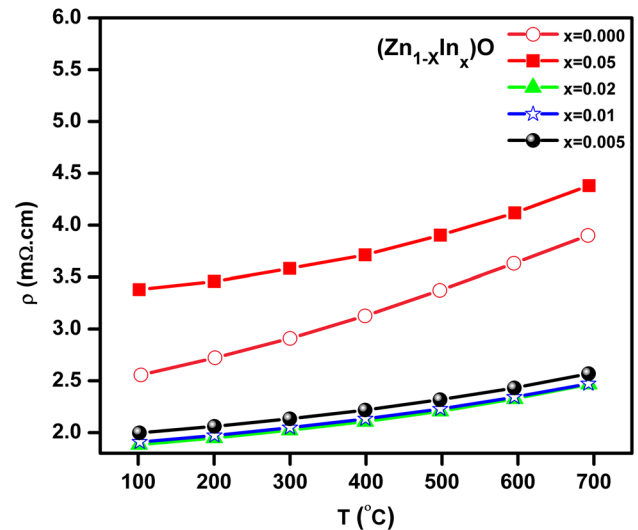
x	c/a	μ
0.00	1.60190	0.37989
0.05	1.60212	0.37986
0.02	1.60374	0.37960
0.01	1.60112	0.38002
0.005	1.60167	0.37993

$$L = \sqrt{\frac{a^3}{3} + \left(\frac{1}{2} - \mu\right)^2 c^2} \quad (2)$$

where a and c are the lattice parameters, while μ is the internal or positional parameter. The optimized bond length for mono structure between Zn and O (ZnO) is 2.21 Å [29]. The μ in wurtzite structure can be calculated by using the equation [30],

$$\mu = \frac{a^2}{3c^2} + 0.25 \quad (3)$$

Figure 4 presents the variation of electrical resistivity (ρ) as a function of temperature. The ρ increases with increase in temperature from 100 to 700 °C. This temperature coefficient of resistivity is positive in this range of temperature. The ρ for the composition with $x=0$ was increased from 2.687 to 3.88 m Ω -cm as the temperature increased from 101.6 to 692.9 °C. The ρ for the composition with $x=0.005$ was increased from 1.997 to 2.568 m Ω -cm as the temperature increased from 101.6 to 692.9 °C. Similarly, for the composition with $x=0.01$, the ρ increased from 1.908 to 2.471 m Ω -cm as the temperature increased from 102.0 to 692.8 °C. For the composition, the ρ was increased from 1.884 to 2.466 m Ω -cm as the temperature increased from 101.4 to 693.4 °C for the composition with $x=0.02$. The ρ was increased from 3.379 to 4.380 m Ω -cm as the temperature increased from 101.3 to 693.7 °C for the composition with $x=0.05$. From this analysis, it is evident that the ρ initially increased from 2.67 to 1.884 m Ω -cm as the x value increased from 0 (zero) to 0.02 and then increased to 3.37 m Ω -cm at 101.3 °C. The reason for the lower ρ of undoped ZnO than the composition with $x=0.05$ is probably due to the lowest number of conduction electrons. Another

**Fig. 4** Temperature dependence of ρ for the nominal formula $(\text{Zn}_{1-x}\text{In}_x)\text{O}$ with $x=0.05$, 0.02, 0.01, 0.005 and 0.00

reason could be the deterioration of the carrier mobility by increased grain boundary scattering and defect scattering. The reason for the increase in ρ with an increase in temperature could be the maximum number of charge carriers, results into the increase in collision among charge carriers in the conduction band. Therefore, in such cases, the semiconductor behaves like a metal [34]. According to Kroing–Vink notation [31],

$$V_o = V_o^* + e^* \quad (4)$$

V_o is the oxygen vacancy, V_o^* is thermal oxygen vacancy and e^* represents the thermally activated electrons or conduction electrons. The number of conduction electrons (e^*) was increased leading a semiconductor to metallic transition (SMT) behavior [33, 34]. For conversion of covalent electrons and holes to conduction electrons about 1.1 eV energy is required [35]. The conduction electrons play an important role in affecting the Seebeck coefficient.

Figure 5 shows the variation in the Seebeck coefficients ($S.C$) of $(\text{Zn}_{1-x}\text{In}_x)\text{O}$ ($x=0.05$, 0.02, 0.01, 0.005 and 0.00) as a function of temperature. All the samples showed negative $S.C$ values indicating n -type conduction and their absolute $S.C$ values increased with increasing temperature due to the thermal excitation of electrons. The $S.C$ has an inverse relation with the number of charge carriers. When the number of charge carriers increases there must be a decrease in the $S.C$ [34]. The undoped ZnO probably possessing a lower number of conduction electrons, these lower number of conduction electrons are responsible for a higher $S.C$. The $S.C$ for undoped ZnO has a maximum value of $-168.28 \mu\text{V K}^{-1}$ at 692.1 °C. The $S.C$ value for $x=0.005$ increases from $-65.51 \mu\text{V K}^{-1}$ to $-106.92 \mu\text{V K}^{-1}$ as the temperature

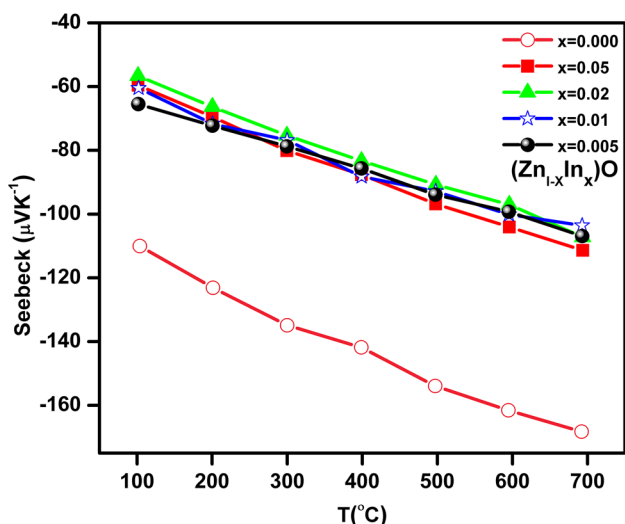


Fig. 5 Temperature dependence of *S.C* for the nominal formula $(Zn_{1-x}In_x)O$, with $x=0.05, 0.02, 0.01, 0.005$ and 0.00

increased from 101.6 to 692.9 °C. The *S.C* value for $x=0.01$ increases from -60.46 to $-103.57 \mu V K^{-1}$ as the temperature increases from 102.0 to 692.8 °C. The *S.C* value for $x=0.02$ increases from -56.62 to $-107.20 \mu V K^{-1}$ as the temperature increased from 101.4 to 693.4 °C. The *S.C* value for $x=0.05$ increases from $-59.60 \mu V K^{-1}$ at 101.3 °C to $-111.36 \mu V K^{-1}$ at 693.7 °C. The *S.C* value increases linearly with increasing temperature according to Mott’s formula [35]. If the number of charge carrier concentrations is high then the value of *S.C* will be decreased as [36],

$$S = \frac{-k_B}{e} \left(\lg \left(\frac{N_c}{n} + A \right) \right) \tag{5}$$

where κ_B is the Boltzmann constant, n is the charge carrier concentration, N_c is the density of states and A represents the transport constant. According to this, carrier concentration (n) is inversely proportional to *S.C* value.

Figure 6 shows the *P.F* of $(Zn_{1-x}In_x)O$ ($x=0.05, 0.02, 0.01, 0.005$ and 0.00) ceramics as a function of temperature. The *P.F* which depends on *S.C* and ρ , is responsible to regulate the electrical properties and is therefore depended on temperature. The higher value of *S.C* and lower values of ρ results in a higher *P.F*. Power factor (*P.F*) is given by [37],

$$P.F = S^2 \sigma \tag{6}$$

Since ρ is lower and *S.C* is higher for the composition with $x=0$ in comparison to $x=0.05$, therefore, it has higher *P.F* value $\sim 7.261 \times 10^{-4} WK^{-2} m^{-1}$ at 692.1 °C. For $x=0.005$, the *P.F* increased from 2.149×10^{-4} to $4.451 \times 10^{-4} WK^{-2} m^{-1}$ with an increase in temperature from 101.6 to 692.9 °C. The *P.F* for $x=0.01$ increased from 1.916×10^{-4} to $4.340 \times 10^{-4} WK^{-2} m^{-1}$ with an

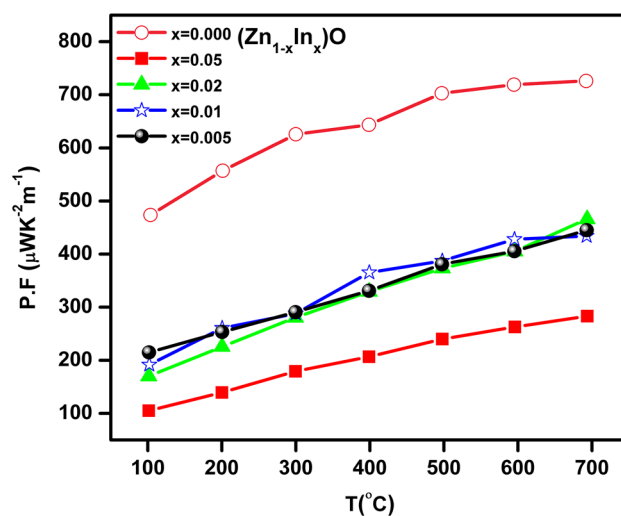


Fig. 6 Temperature dependence of *P.F* for the nominal formula $(Zn_{1-x}In_x)O$, with $x=0.05, 0.02, 0.01, 0.005$ and 0.00

increase in temperature from 102.0 to 692.8 °C. The *P.F* for the sample with $x=0.02$ increased from 1.702×10^{-4} to $4.660 \times 10^{-4} WK^{-2} m^{-1}$ as the temperature increased from 101.4 °C to 693.4 °C. The *P.F* for $x=0.05$ increased from 1.051×10^{-4} to $2.831 \times 10^{-4} WK^{-2} m^{-1}$ as the temperature increased from at 101.3 to 693.7 °C. A higher *P.F* and lower thermal conductivity (σ) are necessary for the better performance of a semiconductor.

Figure 7 presents the changes in *S.C* and ρ of $(Zn_{1-x}In_x)O$, where ($x=0.05, 0.02, 0.01, 0.005$ and 0.00) as a function of In content. It is evident from the results showed in Fig. 7 that *S.C* and ρ has an inverse relation. The highest *S.C* and lowest ρ were observed for the composition with $x=0.02$. For all compositions the *S.C*, *P.F* and ρ were measured at 700 °C.

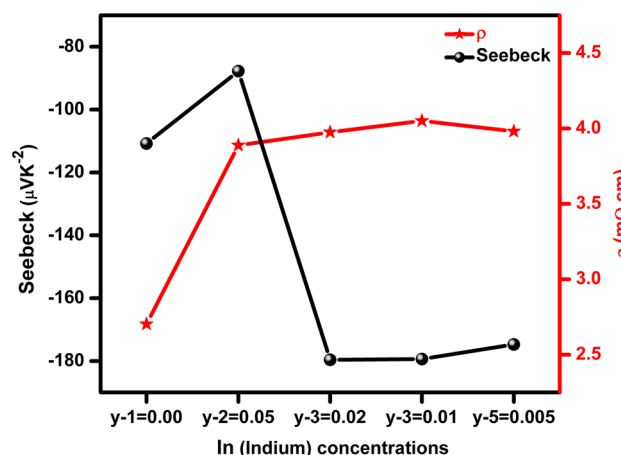


Fig. 7 Relation between *S.C* and ρ for $(Zn_{1-x}In_x)O$, with $x=0.05, 0.02, 0.01, 0.005$ and 0.00

4 Conclusions

Indium-doped ZnO samples have been prepared using flow of argon during sintering at 1450 °C. The as-prepared samples thermoelectric properties, phase, and microstructures were investigated at high temperature ~700 °C under helium atmosphere. A single phase with dense microstructure was observed for each composition. The electrical resistivity (ρ) of ZnO ceramics has lowered by In³⁺ doping. The lowest $\rho \sim 1.884 \text{ m}\Omega\cdot\text{cm}$ and highest $PF \sim 4.660 \times 10^{-4} \text{ WK}^{-2} \text{ m}^{-1}$ at 693.4 °C was obtained for the composition with $x = 0.02$ i.e. (Zn_{0.98}In_{0.02})O.

Acknowledgements The authors acknowledge the support by the Key Laboratory of Advanced Materials and State Key Laboratory of Crystal Materials, Shandong University. The financial support provided by the Government of P. R. China under the Fundamental Research Grant (No. 2015TB019), Jinan 250100, People's Republic of China is also highly acknowledged. The help of professor Ikram Ullah Khan of Government Degree College Bakshali, Mardan, Mardan 23200, Khyber Pakhtunkhwa, Pakistan for his valuable discussion and English language improvements is also highly acknowledged.

References

1. A. Janotti, C.G. Van de Walle, Rep. Prog. Phys. **72**, 126501 (2009)
2. G. Liu, T. Wang, Acta Chim. Sin. **75**(11), 1029 (2017)
3. N. Liu, Z. Li, Mater. Sci. Semicond. Process. **79**, 24 (2018)
4. L. E. Bell, Science **321**, 1457 (2008)
5. R.U.R. Sagar, X. Zhang, C. Xiong, Y. Yu, Carbon **76**, 64 (2014)
6. K. Qiu, A. Hayden, Appl. Energy **91**, 304 (2012)
7. A.Z. Sahin, B.S. Yilbas, S.Z. Shuja, O. Momin, Energy **36**, 4048 (2011)
8. C.H. Kwon, H.K. Hong, D.H. Yun, K. Lee, S.T. Kim, Sen. Actuators B **25**, 610 (1995)
9. T.K. Roy, D. Sanyal, D. Bhowmick, A. Chakrabarti, Mater. Sci. Semicond. Process **16**, 332 (2013)
10. A. Janotti, C.G. Vande Walle, Phys. Rev. B **76**, 165202 (2007)
11. P.D.C. King, T.D. Veal, J. Phys.: Condens. Matter. **23**, 334214 (2011)
12. S. Dutta, S. Chattopadhyaya, A. Sarkar, M. Chakrabarti, D. Sanyal, D. Jana, Prog. Mater. Sci. **54**, 89 (2009)
13. B. Shabbir, X. Wang, Y. Ma, S.X. Dou, S.S. Yan, & L. M. Mei, Sci. Rep. **6**, 23044 (2016)
14. B. Shabbir, X. Wang, S.R. Ghorbani, A.F. Wang, S. Dou, & X. H. Chen, Sci. Rep. **5**, 10606 (2015)
15. B. Shabbir, H. Huang, C. Yao, Y. Ma, S. Dou, T.H. Johansen, H. Hosono, X. Wang, Phys. Rev. Mater. **1**(4), 044805 (2017)
16. B. Shabbir, M. Nadeem, Z. Dai, M.S. Fuhrer, X. Wang, Q. Bao, Appl. Phys. Rev. **5**(4), 041105 (2018)
17. M. Ohtaki, T. Tsubota, K. Eguchi, H. Arai, J. Appl. Phys. **79**, 1816 (1996)
18. S. Yang, F. Chen, X. Gao, Q. Shen, L. Zhang, J. Am. Ceram. Soc. **100**, 1300 (2017)
19. H. Agura, A. Suzuki, T. Matsushita, T. Aoki, M. Okuda, Thin. Sol. Film. **445**, 263 (2003)
20. J. Zhang, W. Zhang, E. Zhao, H. J. Jacques, Mater. Sci. Semi. Proc. **14**, 189 (2011)
21. D. Bérardan, C. Byl, N. Dragoe, J. Am. Ceram. Soc. **93**, 2352 (2010)
22. N. Vogel-Schäuble, Y.E. Romanyuk, S. Yoon, K.J. Saji, S. Populoh, S. Pokrant, Thin Solid Films **520**, 6869 (2012)
23. M. Ullah, C.L. Wang, W.B. Su, A. Zaman, I. Ullah, J.Z. Zhai, D.K. Liu, J. Mater. Sci.: Mater. Electron. **29**, 9555 (2018)
24. M. Ullah, C.L. Wang, W.B. Su, J. Li, A. Manan, I. Ullah, M. Idrees, Mater. Sci. Semicond. Process **87**, 202 (2018)
25. G. Korotcenkov, V. Brinzari, M. H. Ham, Crystals **8**, 1–37 (2018)
26. R.D. Shannon, Acta Crystallogr. A **32**, 751 (1976)
27. B. Karthikeyan, T. Pandiyarajan, K. Mangaiyarkarasi, Spectrochim. Acta A **82**, 97 (2011)
28. S. Singhal, J. Kaur, T. Namgyal, R. Sharma, Phys. B: Cond. Mater. **407**, 1223 (2012)
29. X.S. Wang, Z.C. Wu, J.F. Webb, Z.G. Liu, Appl. Phys. A **77**, 561 (2003)
30. D.I. Rusu, G.G. Rusu, D. Luca, Acta Phys. Pol. A **119**, 850 (2011)
31. T. Norby, J. Korean Ceram. Soc. **47**(1), 19 (2010)
32. Q. Wan, Q.H. Li, Y.J. Chen, T.H. Wang, X.G. He, Gao, J.P. Li, Appl. Phys. Lett. **84**, 3085 (2004)
33. K. Vanheusden, C.H. Seager, W.L. Warren, D.R. Tallant, J.A. Voigt, Appl. Phys. Lett. **68**(3), 403 (1996). <https://doi.org/10.1063/1.116699>
34. A.M. Alsmadi, N. Masmali, H. Jia, J. Guenther, H.A. Jeib, L.L. Kerr, & K. F. Eid, J. Appl. Phys. **117**, 155703 (2015)
35. N.F. Mott, Philos. Mag. **26**, 1015 (1972)
36. H. Cheng, X.J. Xu, H.H. Hng, J. Ma, Ceram. Int. **35**, 3067 (2009)
37. M. Ullah, W.B. Su, A. Manan, A. S. Ahmad, Z. A. A. Shah, Z. Yao, Ceram. Int. **44**(15), 17873 (2018)